Vibrational−Torsional Excitation and Direct Overtone Photodissociation of Ethyl Hydroperoxide at $5\nu_{OH}$

Kristina D. Closser,[†] Kristen M. Vogelhuber,[‡] and Shizuka Hsieh*

Department of Chemistry, Clark Science Center, Smith College, Northampton, Massachusetts 01063

Received: August 24, 2007; In Final Form: October 27, 2007

We have observed OH radical products from the unimolecular dissociation of ethyl hydroperoxide (CH_3CH_2OOH) excited to $5\nu_{OH}$ and have collected an action spectrum from 15 600 to 16 800 cm^{-1} and an OH product state distribution at the maximum (16 119 cm^{-1}). We use a vibrational−torsional model to simulate spectra in the $5\nu_{OH}$ region for the trans and gauche conformers. A combination of the two simulated spectra resembles the experimental action spectrum, provided that the trans conformer is assumed to dominate at room temperature. Energy disposal in the OH fragment yields an upper limit for the O−O bond dissociation energy at $D_0 < 44$ kcal mol^{-1}.

1. Introduction

Organic hydroperoxides such as methyl and ethyl hydroperoxide (CH_3OOH and CH_3CH_2OOH) are byproducts of hydrocarbon oxidation via the reaction of alkyl peroxy radicals with hydroperoxyl radicals (HO_2).[1−3] Their ultraviolet photochemistry involves cleavage of the weak O−O bond to form hydroxyl radicals (OH).[4−8] At lower photon energies, visible light can also form OH radicals via direct overtone photodissociation (Figure 1), as has been observed for *tert*-butyl hydroperoxide at $5\nu_{OH}$[9] and $6\nu_{OH}$[10,11] and more recently for CH_3OOH at $4\nu_{OH}$[12] and $5\nu_{OH}$.[8,12,13] Dissociation at $4\nu_{OH}$ becomes possible in part because of a relatively low dissociation energy for the O−O bond in CH_3OOH, $D_0 = 42.6 \pm 1$ kcal mol^{-1},[13] in comparison with earlier predictions at 45 kcal mol^{-1}.[14]

Yet the O−O bond is strong enough that the O−H overtone excitation energy at $4\nu_{OH}$ (13 285 cm^{-1}, 38 kcal mol^{-1}) alone is not enough to cause OH radical formation. A second key to this below-threshold dissociation is in the nature of vibrations excited in O−H stretch overtone regions. The vibrational overtone spectra of hydroperoxides show not only features due to the O−H stretch but also torsional excitation about the O−O bond.[15,16] At $4\nu_{OH}$, the CH_3OOH molecules that dissociate are ones with additional energy from a combination of thermal and torsional excitation. Using a simple count of vibrational and rotational states[17] along with our simulated spectra,[12,18] we estimate that, at room temperature, only 2−3% of absorption at $4\nu_{OH}$ can lead to dissociation. Of the fraction of molecules that can dissociate, an estimated >75% are in torsionally excited states, underlying the role of torsion in the direct overtone photodissociation of organic hydroperoxides.

Given the importance of both the O−O bond dissociation energy D_0 and the vibrational−torsional transitions to CH_3OOH direct overtone dissociation, we set out to provide an experimental D_0 and to characterize vibrational−torsional excitation for CH_3CH_2OOH. To our knowledge, this is the first report of OH radical formation from the overtone excitation of CH_3CH_2OOH.

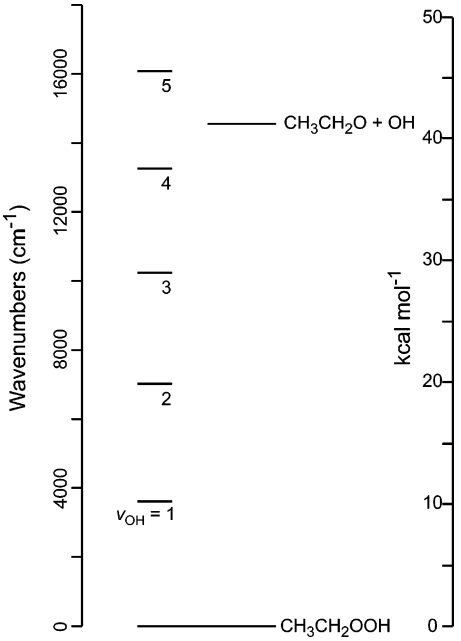

Figure 1. Energy level diagram for the direct overtone dissociation of ethyl hydroperoxide. Energies are relative to the vibrational zero point energy. The dissociation energy (41.6 kcal mol^{-1}) shown here is the calculated value from Hou et al.[3]

Unlike the previously studied organic hydroperoxides (CH_3OOH and *tert*-butyl hydroperoxide), CH_3CH_2OOH has two stable conformers due to differences in the dihedral angle about the C−O bond (Figure 2). Earlier work labels them as STS and SGS,[19] where the initial S indicates a staggered geometry about the C−C bond and the final S indicates a skewed geometry about the O−O bond. The dihedral angle about the C−O bond is either 180° for a trans geometry in STS or near 60° for a gauche conformation in SGS. The potential barrier for torsion about the C−O bond separating the two conformers is on the order of 3 kcal mol^{-1}.[19] Lay et al. consider the two conformers to have very similar potential energies. Their HF/6-31G*

* Corresponding author. E-mail: shsieh@email.smith.edu.
[†] Department of Chemistry, University of California, Berkeley, CA 94720.
[‡] Department of Chemistry and Biochemistry, University of Colorado, Boulder, CO 80309.

10.1021/jp076803r CCC: $40.75
Published on Web 01/23/2008

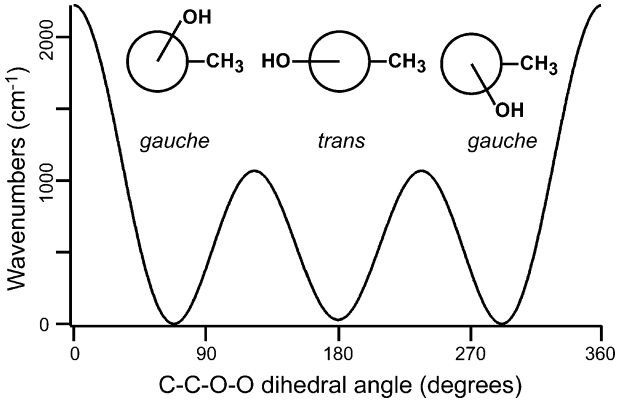

Figure 2. Torsional potential about the C−O bond with wells corresponding to the stable conformers of ethyl hydroperoxide. The torsional potential is taken from Lay et al.,[19] whose MP2/6-31G* calculations indicate the gauche conformer to be more stable.

calculations place STS lower in energy by 0.38 kcal/mol, while MP2/6-31G* calculations show STS to be 0.08 kcal/mol higher in energy.[19] More recent B3LYP/6-311G(d,p) calculations show the optimized geometry of CH_3CH_2OOH to be in the trans conformation.[3] This work provides experimental confirmation that the trans isomer is the more stable of the two conformers.

2. Experimental Section

Detection of OH radicals from CH_3CH_2OOH required two dye lasers, the pump beam for which was 532 nm light from a pulsed Spectra Physics LAB-150 operating at 10 Hz with pulses of 9−10 ns FWHM (manufacturer-specified). A portion of the 532 nm light (220 mJ pulse^{-1}) pumped a Sirah Cobra Stretch dye laser to generate the overtone-excitation light (∼65 mJ pulse^{-1}, manufacturer-specified line width 0.04 cm^{-1} near 630 nm), which was focused into the middle of the gas cell. The other portion of the 532 nm radiation (120 mJ pulse^{-1}) pumped a Sirah Cobra dye laser that output ∼615 nm (∼12 mJ pulse^{-1}, manufacturer-specified line width 0.07 cm^{-1} near 620 nm). For both lasers, the dyes were mixtures of rhodamine 610, rhodamine 640, and DCM. An INRAD Autotracker III doubled the ∼615 nm light to generate the OH probe light, and UG-11 glass filtered out the fundamental before the probe light reached the gas cell. UV filters kept powers below 8 μJ pulse^{-1}, measured just before the gas cell, to maintain linear dependence of the signal on probe powers and to prevent saturation. An optical delay spaced the peak of the OH probe 11 ns after the overtone-excitation pulse peak. A power meter placed after the gas cell monitored the relative power of the overtone-excitation pulse; a photodiode before the gas cell monitored that of the probe pulse by detecting scattered UV light. We verified linear dependence of the laser-induced fluorescence (LIF) signal, described in more detail below, on both laser beam powers and normalized signals for variations in laser powers accordingly.

The laser beams entered the glass gas cell collinearly. The gas cell had baffles in the arms and a photomultiplier tube (Electron Tubes 9235QB) located perpendicular to the laser beams and above the focal point of the overtone excitation beam. Two lenses (77.5-mm focal length) imaged the LIF onto the photomultiplier tube, and a UG-11 filter reduced visible scattered light. The gated fluorescence signal was integrated and collected as a function of laser wavelength, generating two types of spectra. Action spectra came from scanning the overtone-excitation laser; OH rotational distributions came from scanning the probe laser.

Vapor from a ∼7 M aqueous solution of CH_3CH_2OOH flowed through the gas cell at pressures ∼100 mTorr. CH_3CH_2-OOH solutions were synthesized using procedures similar to our previous work.[18] We verified that ethanol and water present in the sample did not contribute to the OH LIF signal.

Experimental OH rotational distributions came from LIF detection using selected transitions in the $A^2\Sigma(v' = 0) \leftarrow X^2\Pi$-$(v'' = 0)$ electronic transition. To ensure no saturation of the OH transitions, we checked that the relative intensities of the $Q_1(2)$ peak and its $Q_{21}(2)$ satellite matched literature[20] values. We collected two sets of line profiles for a range of transitions; data within each set were taken under identical conditions. Since some line profiles contained overlapping peaks, we fit the experimental line profiles with Lorentzian functions. We divided Lorentzian peak areas by Einstein B coefficients[20,21] to determine relative populations. This correction for the transition probability yielded similar results to simulations[22] that took the experimental detection conditions into account. We saw no significant difference in relative populations for P, Q, and R peaks within the same OH electronic and rotational state and, therefore, assumed that there was no significant bias for lambda states at these low rotational quantum numbers (using the notation of Dieke and Crosswhite,[20] $K \leq 9$). Using a combination of P, Q, and R branch data allowed us to avoid specific transitions that had interference from surrounding overlapping peaks. Data within each set were normalized so that the sum of average relative populations was unity.

3. Calculations

Calculations for simulating vibrational−torsional spectra are similar to those in our previous work[12,18] and early papers showing the effect of methyl group torsion on C−H stretch overtones.[23−25] Adiabatic separation of vibrational and torsional motion yields wavefunctions in terms of the displacement from the equilibrium O−H bond length q and the C−O−O−H dihedral angle χ, respectively.

$$\psi_{v,n} = \psi_v^{\mathrm{Vib}}(q)\psi_{v,n}^{\mathrm{Tor}}(\chi) \quad (1)$$

We use notation where v designates the O−H stretch quantum number and n the torsional quantum number. Our calculations consider transitions from the vibrational ground state ($v'' = 0$) to the fifth O−H stretching overtone ($v' = 5$) involving n' and n'' that correspond to the eight lowest-energy torsional states. We use GAUSSIAN 98[26] at the B3LYP/6-311++G(3d,2p) level of theory unless specified.

3.1. O−H Stretch Vibrational States. The O−H stretch vibrational energies and wavefunctions are solutions for a Morse oscillator, characterized by frequency ω and anharmonicity ωx parameters. Adiabatic separation of vibration and torsion implies that O−H stretch frequency varies with C−O−O−H dihedral angle χ. We determine ω and ωx from Gaussian energies at fixed C−O−O−H dihedral angles (χ = 0−360° in 10° increments). At each χ, we optimize the geometry and, freezing the geometry in all other dimensions, calculate the energy as a function of O−H bond length (r_{OH} = 0.75−1.15 Å in 0.02 Å increments). Fitting these points to a 14th order polynomial expansion of the Morse potential yields ω and ωx.[27] We have chosen this particular range of points and method since they yield ωx values that are reasonably matched to values from a Birge−Sponer treatment using the available experimental overtone frequencies.[16] Table 1 lists the calculated frequency and anharmonicity at the dihedral angle for the globally optimized geometry χ_{opt} for each conformer.

3.2. Torsional States. The torsional energies and wavefunctions are solutions to the Schrödinger equation with the kinetic

TABLE 1: Calculated Morse Parameters for the Two Conformers of Ethyl Hydroperoxide

conformer	χ_{opt} (degrees)	ω (cm^{-1})	ωx (cm^{-1})
trans	111.2	3720	97.0
gauche	111.9	3723	96.8

TABLE 2: Calculated Kinetic Energy Parameters for the Two Conformers of Ethyl Hydroperoxide

conformer	υ	χ_{eq}[a] (degrees)	$\langle r_{OH}\rangle$[b] (Å)	α_0[c] (cm^{-1})	α_1[c] (cm^{-1})
trans	0	109.5	0.983	20.02	0.618
gauche	0	110.7	0.983	19.93	0.587
trans	5	91.9	1.185	14.31	0.696
gauche	5	93.4	1.184	14.25	0.672

[a] Dihedral angle at the minimum of the torsional potential. [b] Average O−H bond length. [c] Kinetic energy parameters based on optimized geometries at fixed $\chi = \chi_{eq}$ and $r_{OH} = \langle r_{OH}\rangle$.

energy and potential operators as follows. As in our previous work, we use the kinetic energy operator defined by Dübal and Crim[15]

$$\hat{E}_k = -\frac{d}{d\chi}(\alpha_0 + \alpha_1 \cos(\chi))\frac{d}{d\chi} \tag{2}$$

where the parameters α_0 and α_1 are based on masses and molecular geometries. For each vibrational level, the molecular geometry is optimized with a fixed dihedral angle χ and O−H bond length r_{OH} chosen to account for changes that accompany vibrational excitation (Table 2). The torsional potential $V(\chi)$ for each vibrational level υ includes contributions from the electronic energy V_{elec}, the sum of zero point energies $E_{ZPE'}$ for all modes except for the O−H stretch and torsion, and the O−H stretch vibrational energy.

$$V_\upsilon(\chi) = V_{elec}(\chi) + E_{ZPE'}(\chi) + \omega\left(\upsilon + \frac{1}{2}\right) - \omega x\left(\upsilon + \frac{1}{2}\right)^2 \tag{3}$$

Electronic energies and the vibrational frequencies used to determine $E_{ZPE'}$ come from Gaussian optimizations at fixed values of χ. The Morse parameters ω and ωx, described in section 3.1 above, determine the O−H stretch vibrational energy. We evaluate the potential at $\chi = 0-360°$ in 10° increments and express all energies relative to the electronic energy of the optimized lower energy trans conformer. We fit the points of the resulting potentials to the following Fourier series

$$V(\chi) = V_0 + \sum_{i=1}^{6} V_i \cos(i\chi) + \sum_{j=1}^{3} V_{j+6} \sin(j\chi) \tag{4}$$

The potential is similar to that used in our previous work, except that the additional sine terms are necessary for potentials that are asymmetric about $\chi = 180°$. Figure 3 shows the resulting fits for the $\upsilon = 0$ and $\upsilon = 5$ potentials, and Table 3 lists the fit coefficients.

We find solutions using first-order perturbation theory and a twenty-term basis set of cosines and sines ($\cos(i\chi)$ with $i = 0-9$ and $\sin(j\chi)$ with $j = 1-10$). We take the unperturbed system to be a symmetric potential that contains the cosine terms in eq 4, and the perturbation includes the three sine terms. Since the trans conformer has a symmetric torsional potential about $\chi = 180°$, no perturbation is required. Its wavefunctions are either symmetric or antisymmetric about $\chi = 180°$, so a basis set of cosines ($\cos(i\chi)$ with $i = 0-9$) alone is sufficient for the symmetric wavefunctions, and a basis set of sines ($\sin(j\chi)$ with $j = 1-10$) is sufficient for the antisymmetric wavefunctions.

TABLE 3: Coefficients for C−O−O−H Torsional Potentials for the Two Conformers of Ethyl Hydroperoxide

	trans, $\upsilon = 0$	gauche, $\upsilon = 0$	trans, $\upsilon = 5$	gauche, $\upsilon = 5$
V_0	18669.4	18776. 6	34286.7	34436.9
V_1	785.7	901.6	512.9	653.9
V_2	528.6	573.4	663.0	697.2
V_3	84.6	74.2	174.4	144.0
V_4	15.9	13.6	49.2	39.4
V_5	6.1	4.6	14.7	14.3
V_6	0.3	0.8	0.9	4.9
V_7	0	−41.8	0	−99.4
V_8	0	−27.5	0	−84.8
V_9	0	−11.8	0	−31.6

For the trans conformer, using twenty-term basis sets of cosines or sines alone does not change the results.

3.3. Intensity Calculations. To calculate absorption cross sections, we evaluate the standard expression, here given in units of cm^2 $molecule^{-1}$ cm^{-1},

$$\sigma = \frac{fe^2}{4m_e c^2 \epsilon_0} \tag{5}$$

where f is the unitless oscillator strength for a transition,[28]

$$f_{e\leftarrow g} = 4.70165 \times 10^7 [\text{cm D}^{-2}]\tilde{\nu}_{e\leftarrow g}|\mu_{e\leftarrow g}|^2 \tag{6}$$

for each vibrational−torsional transition. The transition moment in this case is a function of both the O−H bond displacement q and the torsional angle χ

$$\mu_{\upsilon,n'\leftarrow 0,n''} = \sum_k \langle \psi_\upsilon^{Vib}(q,\chi)\psi_{\upsilon,n'}^{Tor}(\chi)|\hat{\mu}_k(q,\chi)|\psi_0^{Vib}(q,\chi)\psi_{0,n''}^{Tor}(\chi)\rangle \tag{7}$$

where $\hat{\mu}(q,\chi)$ is the transition moment operator

$$\hat{\mu}(q,\chi) = \sum_{i=1}^{6} q^i \frac{1}{i!}\left(\frac{d^i\mu(q,\chi)}{dq^i}\right)_{q=0} \tag{8}$$

and $k = (x, y, z)$ denotes its components along the conformer's rotational axes.

The dipole moment operator at each torsional angle (taken every 10° increment starting at $\chi = 0°$) comes from calculating the x, y, and z components of the dipole moment at the HF/6-31G(d) level of theory[29] over a range of OH bond lengths (r_{OH} = 0.65−1.35 Å in 0.05 Å increments) while holding the remainder of the molecule in its HF optimized geometry. We fit each set of calculated dipole moments to a sixth-order[30] polynomial function of q and evaluate the derivatives at $q = 0$. The derivatives, along with the Morse vibrational wavefunctions defined by the frequency ω and anharmonicity ωx at each χ, generate points for an effective dipole moment function

$$\mu_k^i(\chi) = \frac{1}{i!}\langle \psi_\upsilon^{Vib}(q)|q^i|\psi_0^{Vib}(q)\rangle_\chi\left(\frac{d^i\mu_k}{dq^i}\right)_{q=0,\chi} \tag{9}$$

Interpolation to estimate intermediate values and fitting these interpolated points to a twenty-term Fourier series generates functions of χ that are used to calculate the transition moment

$$\mu_{\upsilon,n'\leftarrow 0,n''} = \sum_k \left(\sum_{i=1}^{6} \langle \psi_{\upsilon,n'}^{Tor}(\chi)|\mu_k^i(\chi)|\psi_{0,n''}^{Tor}(\chi)\rangle\right) \tag{10}$$

For our spectral simulations, we multiply the calculated intensities by the Boltzmann population of the initial torsional

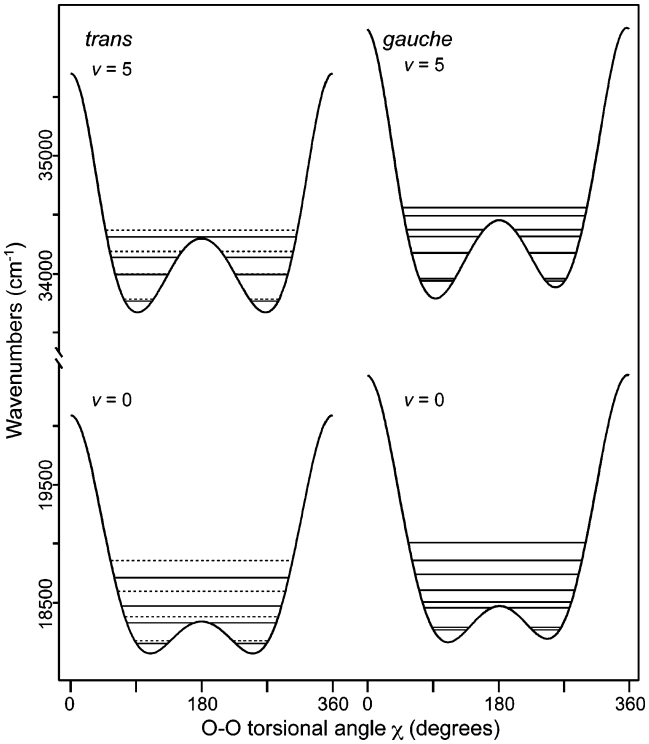

Figure 3. Torsional potentials for the trans (left) and gauche (right) conformers for the excited ($v = 5$, top) and ground (bottom) OH vibrational states. Energies are relative to the electronic energy minimum of the trans conformer. For the trans conformer's torsional energy levels, solid lines indicate states symmetric about $\chi = 180°$ and dotted lines antisymmetric ones.

state at 298 K. To approximate rotational structure, we convolute the weighted cross sections with 50 cm^{-1} FWHM Gaussians.

4. Results and Discussion

4.1. Calculations for Trans and Gauche Conformers. B3LYP/6-311++G(3d,2p) calculations place the trans conformer 86 cm^{-1} lower in electronic energy than the gauche. Adding their calculated zero-point energies (using the fitted potentials described in section 3.2) increases the energy difference to 116 cm^{-1} (0.3 kcal mol^{-1}). Calculations predict therefore that both conformers should be present in a room-temperature sample of CH_3CH_2OOH. Given a Boltzmann distribution that counts the gauche conformer degeneracy as 2, the expected 298 K trans-to-gauche populations are nearly equal.

Simulations for the two conformers differ enough (Figure 4a,b) that their features should be distinguishable in an experimental spectrum. Each simulation shows a similar pattern to our previous vibrational−torsional spectra for methyl hydroperoxide,[12,18] starting with a main band that involves only O−H stretch vibrational excitation and no change in torsional quantum number. Calculations, however, place the main bands for the two conformers 60 cm^{-1} apart (at 15 611 cm^{-1} for the trans conformer and at 15 671 cm^{-1} for the gauche), due in part to differences in their calculated O−H stretch vibrational frequencies ω and anharmonicities ωx (Table 1) but mainly to differences in torsional zero-point energies. In general, features to the blue of each main band correspond to transitions involving torsional excitation, and those to the red correspond to hot bands involving a decrease in torsional quantum number. The simulated absorption spectra show relatively more contribution from these torsional features in the trans conformer case.

4.2. Action Spectrum. The features in the action spectrum monitoring the $Q_1(1)$ branch of the OH product share the same

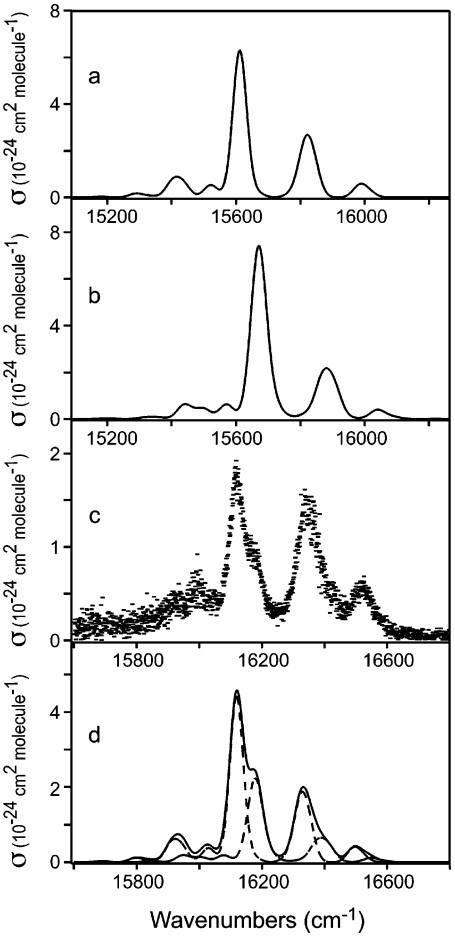

Figure 4. Vibrational−torsional spectra of ethyl hydroperoxide at $5\nu_{OH}$. Simulated absorption spectra for the (a) trans and (b) gauche conformers are shown at the top. Simulations are not weighed for relative populations in a room-temperature sample. The vertical axis of the experimental action spectrum (c) is a scaled match to the absorption cross section from our previous work.[16] Shifting the simulated spectra 507 cm^{-1} to the blue and summing weighted contributions from the two conformers (dotted lines) yields the solid line in (d).

relative intensities as those in our published photoacoustic spectrum.[16] Scaling the action spectrum to the published experimental cross section[16] yields Figure 4c. The similarity between the action and the photoacoustic spectra indicates no preferential formation of OH from specific vibrational−torsional states in the $5\nu_{OH}$ region.

The experimental action spectrum bears closer resemblance to the calculated absorption spectrum for the trans conformer, but a combination of the two simulated spectra generates a more compelling match to the experimental data. Shifting both simulated spectra 507 cm^{-1} to the blue and giving them relative trans/gauche contributions of 0.7:0.3 yields a summed simulation (Figure 4d) that resembles the experimental action spectrum.

This summed simulation is consistent with the trans conformer dominating in a room-temperature sample. In principle, the simulation could also be used to determine an experimental energy difference between the two conformers via the population ratio that yields the best match to the data. A trans/gauche Boltzmann population ratio of 0.7:0.3 at 298 K, for example, corresponds to the trans conformer lying ~300 cm^{-1} (0.9 kcal mol^{-1}) lower in summed electronic and zero-point energy. This value should be taken with caution, however, since the simulation does not make a perfect match to the data and since higher-level cross section calculations are likely to change the appropriate population ratio for the simulation. Since one-

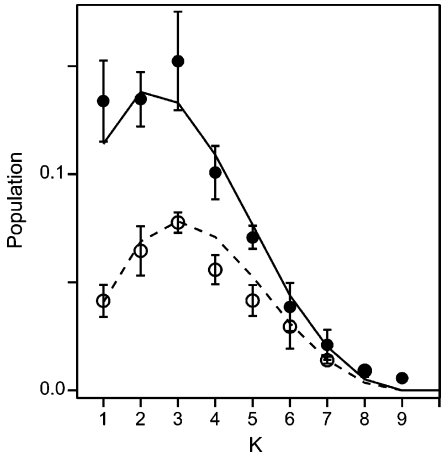

Figure 5. OH fragment rotational distribution from ethyl hydroperoxide direct overtone dissociation at $5\nu_{OH}$, as observed (circles) and predicted using a prior distribution (lines). The solid circles and lines are for the $^2\Pi_{3/2}$ states and open (or dotted) for $^2\Pi_{1/2}$. Following the notation in ref 20, the quantum number K indicates the angular momentum excluding the electron spin.

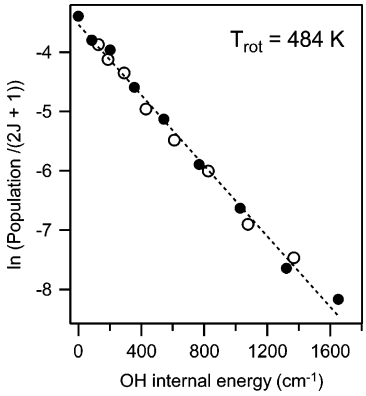

Figure 6. OH fragment rotational temperature from direct overtone dissociation of ethyl hydroperoxide at $5\nu_{OH}$. The solid circles are for the $^2\Pi_{3/2}$ states, and open circles are for $^2\Pi_{1/2}$.

dimensional calculations that ignore the dipole moment's and vibrational wavefunctions' dependence on torsional angle in eq 7 give similar results, as was the case in our previous work,[12] we can also make a comparison with one-dimensional cross sections determined using a higher level of theory (B3LYP/aug-cc-PVTZ) and a different method for determining Morse parameters.[31] For these additional calculations,[32] slightly different methods than ours are also used to determine dipole moment functions.[30] With this set of integrated cross sections, generating a similar simulation to Figure 4d requires a trans/gauche ratio closer to 0.6:0.4, which corresponds to a ~250 cm^{-1} energy difference between the two conformers. These values are closer to the calculation predictions from section 4.1.

Assigning the shoulder to the blue of the main peak as a gauche conformer feature revises our earlier interpretation,[16] where we had assumed it to be a hot band from the trans conformer. While the calculations do show a hot band for a transition from the first excited symmetric torsional state (S_1^1 in the notation of our earlier work) located 53 cm^{-1} to the blue of the main peak, its intensity is weak enough (<6% of the S_0^0 contribution to the main peak) that it does not appear as a distinct feature in the simulation (Figure 4a).

4.3. Rotational Energy Partitioning in the OH Fragment. Figure 5 shows the distribution of nascent OH rotational states at an overtone excitation energy of 16 119 cm^{-1}, which corresponds to the maximum in the action spectrum. The populations follow a Boltzmann distribution at $T_{rot} = 484$ K (Figure 6). Energetic constraints (Figure 1) prohibit the formation of vibrationally excited OH fragments in the unimolecular dissociation of CH_3CH_2OOH at $5\nu_{OH}$. The average internal energy for the OH fragment comes therefore from the distribution in Figure 5 and is 329 ± 17 cm^{-1}.

The experimental distribution resembles predictions using simple statistical models (Figure 5). We consider the prior model and phase space theory (PST).[33] The prior model counts all combinations of product quantum states that are energetically possible and assumes them to be equally probable. In its simplest form, PST also counts all product states as equally probable, with the addition of an angular momentum constraint that depends on the initial CH_3CH_2OOH rotational quantum number J. Since calculations even for a molecule as small as HOOH show similar product state distributions over a range of initial J_{HOOH} states,[34] we limit our PST treatment to the average J state for the trans conformer at room temperature, $J_{CH_3CH_2OOH} = 36$, as determined by treating it as a prolate symmetric top with the Gaussian calculated rotational constants ($A = 1.04$ cm^{-1} and $B = 0.134$ cm^{-1}, which is the average of its asymmetric rotor constants $B = 0.138$ cm^{-1} and $C = 0.129$ cm^{-1}).

Further details of our calculations are as follows. For OH, we consider the $f_1(K)$ and $f_2(K)$ states[20] but do not include their respective lambda doublets. We treat CH_3CH_2O as a symmetric prolate top, using rotational constants from the literature.[35] The direct count of harmonic vibrational states uses CH_3CH_2O frequencies from Zhu et al.[36] Since a full list of literature values is not available for CH_3CH_2O's low-lying A electronic state, which is only 355 cm^{-1} above the ground state,[37] we use the same frequencies for it. We consider this approximation to have an insignificant effect on the results for two reasons. First, neglecting the A state altogether only leads to a slight overestimate for the population of high J_{OH} states, with differences in population typically less than ~0.003. Second, a similar treatment of CH_3OOH dissociation also leads to similarly small differences (typically <0.004) when using known CH_3O A state frequencies.[38] For the internal energy of CH_3CH_2OOH, we assume the Gaussian-calculated thermal value for the trans conformer, $E_{thermal} = 895$ cm^{-1}. Finally, we leave the dissociation energy D_0 as an adjustable parameter.

For this relatively large molecule at room temperature, the prior model and PST, not surprisingly, give similar results. The only difference is that the PST angular momentum constraint effectively reduces the probability of forming CH_3CH_2O states with high J and high degeneracy. Since these high J states are only energetically accessible in combination with low J_{OH} states, the reduction affects low J_{OH} populations more strongly. As a result, PST populations are slightly hotter than the prior predictions. With the high average $J_{CH_3CH_2OOH}$ for a room-temperature sample, the effect is small, and our PST and prior population differences are typically less than ~0.002.

Since the results are so similar for both statistical models, we show the simpler prior distribution, using $D_0 = 44$ kcal mol^{-1}, against the experimental data in Figure 5. It is not surprising that statistical models provide good agreement with the data since PST has had some success for the direct overtone dissociation of even smaller molecules, such as HOOH[34,39,40] and $HONO_2$.[41] For example, PST predictions follow experimental distributions well for state-resolved dissociation from specific rotational states within the $6\nu_{OH}$ and $4\nu_{OH} + \nu_{OH}$ HOOH overtone states.[40] However, it overestimates populations of high J_{OH} states from $5\nu_{OH} + \nu_{OO}$ and $5\nu_{OH} + \nu_{OOH}$.[40] For $HONO_2$ at $5\nu_{OH}$ and $6\nu_{OH}$, PST predictions match experiments, with the

exception of relative populations of spin−orbit states from dissociation at $6\nu_{OH}$.[41]

Our prior distributions for CH_3CH_2OOH are sensitive to input D_0 values. For example, changing D_0 by ±1 kcal mol^{-1} shifts populations by <0.015, increases the sum of residuals by ~25%, and provides qualitatively worse fits to the data. However, we regard the value used in our prior distribution (Figure 5) only to be an upper limit to the actual dissociation energy. We base our reasoning on the fact that similar calculations also give good qualitative agreement with CH_3OOH data from Matthews et al.[13] (not shown), but only when the dissociation energy is assumed to be $D_0 \sim 44.5$ kcal mol^{-1}, which is 2 kcal mol^{-1} above their reported value. Below, we show that this estimate from our statistical calculations ($D_0 < 44$ kcal mol^{-1}) is consistent with the measured value.

4.4. O−O Bond Dissociation Energy D_0. The overtone excitation photon imparts $E_{h\nu} = 16\,119$ cm^{-1} to room-temperature molecules that, as mentioned above, have an estimated internal energy $E_{thermal} = 895$ cm^{-1} at 298 K. Upon dissociation, some of that energy goes into dissociation D_0, while the rest goes into translational energy and internal energy of the two fragments.

$$E_{h\nu} + E_{thermal} = D_0 + E_{trans} + E_{int}(OH) + E_{int}(CH_3CH_2O)$$

Determining the O−O bond dissociation energy D_0 requires a complete description of energy disposal. While we cannot determine the CH_3CH_2O internal energy, we can estimate the translational energy. Our Doppler profiles for CH_3CH_2OOH dissociation are identical to ones we obtain from the direct overtone dissociation of CH_3OOH at 16 142 cm^{-1}. The literature total kinetic energy release for CH_3OOH dissociation at that photon energy is ~1400 cm^{-1}.[13] An identical kinetic energy for the OH fragment corresponds to a lower total kinetic energy release ~1250 cm^{-1} for CH_3CH_2OOH dissociation. Combining $E_{trans} = 1250$ cm^{-1} with the average rotational energy (329 ± 17 cm^{-1}) for E_{int}(OH) yields an upper limit for the dissociation energy $D_0 < 44.1$ kcal mol^{-1}. A second estimate for D_0 comes from assuming that the highest rotationally excited OH fragments are accompanied by negligible translational and CH_3CH_2O internal energies. The highest rotationally excited OH fragment we observe is in the $f_1(9)$ state, which has an internal energy of 1651 cm^{-1}. Using this value for E_{int}(OH) also yields an upper bound for the dissociation energy at $D_0 < 43.9$ kcal mol^{-1}. Neither experimental value of D_0 takes into account the internal energy of the CH_3CH_2O fragment. If it has a similar vibrational and rotational temperature to the OH fragment's rotational temperature ($T_{rot} \sim 484$ K, Figure 6), its internal vibrational energy would be ~530 cm^{-1}, and its internal rotational energy would be 510 cm^{-1}. Subtracting this estimated internal energy for the ethoxy radical yields $D_0 \sim 41.1$ kcal mol^{-1}. This experimental value compares favorably with $D_0 = 41.6$ kcal mol^{-1}, which comes from RCCSD(T)/CBS enthalpies of formation[3] for the reactants and products in the following reaction.

$$CH_3CH_2OOH + O_2 \rightarrow CH_3CH_2O + OH + O_2$$

Those same calculations predict a dissociation enthalpy of $\Delta H_{298} = 43.0$ kcal mol^{-1}. In comparison, experimental enthalpies of formation in the literature[42] yield $\Delta H_{298} = 46.7 \pm 3.2$ kcal mol^{-1}.

5. Conclusions

We demonstrate OH product formation in the direct overtone photodissociation of CH_3CH_2OOH at $5\nu_{OH}$. Monitoring the OH yield as a function of wavelength yields an action spectrum in the $5\nu_{OH}$ region (15 600 to 16 800 cm^{-1}) that mimics the published photoacoustic spectrum.[16] A vibrational−torsional model successfully predicts features in the action spectrum and provides insight into the relative stabilities of the CH_3CH_2OOH trans and gauche conformers. Interpreting the action spectrum as a mixture of contributions from the two is consistent with the trans conformer dominating in a room-temperature sample.

The experimental energy disposal places an upper bound on the O−O bond dissociation energy at $D_0 < 44$ kcal mol^{-1}. Our measurement is in agreement with a recent calculated value, $D_0 = 41.6$ kcal mol^{-1},[3] supporting the prediction[3] that the dissociation enthalpy ΔH_{298} is ~3.7 kcal mol^{-1} lower than current experimental enthalpies of formation in the literature indicate ($\Delta H_{298} = 46.7 \pm 3.1$ kcal mol^{-1}).[42] Such low O−O bond dissociation energies might make direct overtone dissociation accessible for thermally excited organic hydroperoxides at $4\nu_{OH}$, as we have already observed for CH_3OOH.[12]

Acknowledgment. We thank Kimberly R. Kufel and Kristin M. Wilson for assistance with some of the experiments. Smith College and ACS/PRF (#42568-GB6) funded this work, and HHMI funded the Early Mentoring Program at Smith College that supported both Kufel and Wilson. S.H. thanks Professor Amy Mullin and the University of Maryland, College Park, MD for hosting her as a visiting scientist. S.H. also thanks Professor Henrik Kjaergaard for helpful discussions and some additional calculations.

References and Notes

(1) Wallington, T.; Japar, S. *Chem. Phys. Lett.* **1990**, *166*, 495.
(2) Hasson, A.; Tyndall, G.; Orlando, J. *J. Phys. Chem. A* **2004**, *108*, 5979.
(3) Hou, H.; Li, J.; Wang, B. *J. Phys. Chem. A* **2005**, *109*, 11206.
(4) Vaghjiani, G. L.; Ravishankara, A. R. *J. Chem. Phys.* **1990**, *92*, 996.
(5) Roehl, C. M.; Marka, Z.; Fry, J. L.; Wennberg, P. O. *Atmos. Chem. Phys.* **2007**, *7*, 713.
(6) Ryu, B.-G.; Park, C. R.; Lee, Y.; Shin, S. K.; Kim, H. L. *J. Photochem. Photobio. A* **2002**, *149*, 15.
(7) Novicki, S. W.; Vasudev, R. *J. Chem. Phys.* **1990**, *93*, 8725.
(8) Matthews, J.; Sinha, A.; Francisco, J. S. *Proc. Natl. Acad. Sci.* **2005**, *102*, 7449.
(9) Chandler, D. W.; Farneth, W. E.; Zare, R. N. *J. Chem. Phys.* **1982**, *77*, 4447.
(10) Rizzo, T. R.; Crim, F. F. *J. Chem. Phys.* **1982**, *76*, 2754.
(11) Chuang, M.-C.; Baggott, J. E.; Chandler, D. W.; Farneth, W. E.; Zare, R. N. *Faraday Discuss. Chem. Soc.* **1983**, *75*, 301.
(12) Haynes, L. M.; Vogelhuber, K. M.; Pippen, J. L.; Hsieh, S. *J. Chem. Phys.* **2005**, *123*, 234306.
(13) Matthews, J.; Sinha, A.; Francisco, J. S. *J. Chem. Phys.* **2005**, *122*, 21101.
(14) Bach, R. D.; Ayala, P. Y.; Schlegel, H. B. *J. Am. Chem. Soc.* **1996**, *118*, 12758.
(15) Dübal, H.-R.; Crim, F. F. *J, Chem. Phys.* **1985**, *83*, 3863.
(16) Homitsky, S. C.; Dragulin, S. M.; Haynes, L. M.; Hsieh, S. *J. Phys. Chem. A* **2004**, *108*, 9492.
(17) Dorofeeva, O. V.; Noikov, V. P.; Neumann, D. B. *J. Phys. Chem. Ref. Data* **2001**, *30*, 475.
(18) Haynes, L. M.; Vogelhuber, K. M.; Pippen, J. L.; Hsieh, S. *J. Chem. Phys.* **2007**, *126*, 209901.
(19) Lay, T. S.; Krasnoperov, L. N.; Venanzi, C. A.; Bozzelli, J. W.; Shokhirev, N. V. *J. Phys. Chem.* **1996**, *100*, 8240.
(20) Dieke, G. H.; Crosswhite, H. M. *J. Quant. Spectrosc. Radiat. Transfer* **1962**, *2*, 97.
(21) Chidsey, I. L.; Crosley, D. R. *J. Quant. Spectrosc. Radiat. Transfer* **1979**, *23*, 187.
(22) Luque, J.; Crosley, D. R. *LIFBASE*: Database and spectral simulation, Version 1.5; 1999.
(23) Cavagnat, D.; Lascombe, J. *J. Mol. Struct.* **1982**, *80*, 363.
(24) Cavagnat, D.; Lespade, L. *J. Chem. Phys.* **1997**, *106*, 7946.
(25) Zhu, C.; Kjaergaard, H. G.; Henry, B. R. *J. Chem. Phys.* **1997**, *107*, 691.

(26) Frisch, M. J.; Trucks, G. W.; Schlegel, H. B.; Scuseria, G. E.; Robb, M. A.; Cheeseman, J. R.; Zakrewski, V. G.; Montgomery, J. A., Jr.; Stratmann, R. E.; Burant, J. C.; Dapprich, S.; Millam, J. M.; Daniels, A. D.; Kudin, K. N.; Strain, M. C.; Farkas, O.; Tomasi, J.; Barone, V.; Cossi, M.; Cammi, R.; Mennucci, B.; Pomelli, C.; Adamo, C.; Clifford, S.; Ochterski, J.; Petersson, G. A.; Ayala, P. Y.; Cui, Q.; Morokuma, K.; Malick, D. K.; Rabuck, A.; Raghavachari, K.; Foresman, J. B.; Cioslowski, J.; Ortiz, J. V.; Stefanov, B. B.; Liu, G.; Liashenko, A.; Piskorz, P.; Komaromi, I.; Comperts, R.; Martin, R. L.; Fox, D. J.; Keith, T.; Al-Laham, M. A.; Peng, C. Y.; Nanayakkara, A.; Gonzales, C.; Challacombe, M.; Gill, P. M. W.; Johnson, B. G.; Chen, W.; Wong, M. W.; Andres, J. L.; Head-Gordon, M.; Replogle, E. S.; Pople, J. A. *Gaussian 98*, Revision A.6; Gaussian, Inc.: Pittsburgh, PA, 1998.

(27) McQuarrie, D. A.; Simon, J. D. *Physical Chemistry: A Molecular Approach*; University Science Books: Sausalito, 1997.

(28) Atkins, P. W. *Molecular Quantum Mechanics*, 2nd ed.; Oxford University Press: Oxford, 1983.

(29) Daub, C. D.; Henry, B. R.; Sage, M. L.; Kjaergaard, H. G. *Can. J. Chem.* **1999**, *77*, 1775.

(30) Rong, Z.; Kjaergaard, H. G. *J. Phys. Chem. A* **2002**, *106*, 6242.

(31) Howard, D. L.; Jorgensen, P.; Kjaergaard, H. G. *J. Am. Chem. Soc.* **2005**, *127*, 17096.

(32) Kjaergaard, H. G., private communication.

(33) Baer, T.; Hase, W. L. *Unimolecular Reaction Dynamics: Theory and Experiments*; Oxford University Press: Oxford, 1996.

(34) Rizzo, T. R.; Hayden, C. C.; Crim, F. F. *J. Chem. Phys.* **1984**, *81*, 4501.

(35) Tarczay, G.; Gopalakrishnan, S.; Miller, T. A. *J. Mol. Spectrosc.* **2003**, *220*, 276.

(36) Zhu, X.; Kamal, M. M.; Misra, P. *Pure Appl. Optics* **1996**, *5*, 1021.

(37) Ramond, T. M.; Davico, G. E.; Schwartz, R. L.; Lineberger, W. C. *J. Chem. Phys.* **2000**, *112*, 1158.

(38) Powers, D. E.; Pusharsky, M. B.; Miller, T. A. *J. Chem. Phys.* **1997**, *106*, 6863.

(39) Ticich, T. M.; Rizzo, T. R.; Dubal, H.-R.; Crim, F. F. *J. Chem. Phys.* **1985**, *84*, 1508.

(40) Luo, X.; Rizzo, T. R. *J. Chem. Phys.* **1991**, 5129.

(41) Sinha, A.; VanderWal, R. L.; Crim, F. F. *J. Chem. Phys.* **1990**, *92*, 401.

(42) Sander, S. P.; Friedl, R. R.; Golden, D. M.; Kurlyo, M. J.; Moortgat, G. K.; Keller-Rudek, H.; Wine, P. H.; Ravishankara, A. R.; Kolb, C. E.; Molina, M. J.; Finlayson-Pitts, B. J.; Huie, R. E.; Orkin, V. L. Chemical Kinetics and Photochemical Data for use in Atmospheric Studies Evaluation Number 15. In *JPL Publication 06-2*, 2006.